PIER C

(Received 28 May 2024, Accepted 18 July 2024, Scheduled 7 August 2024)

Robust Model Predictive Torque Control with Online Parameter Identification Based on Improved Differential Evolution Extended Kalman Filter for PMSM

Yang Zhang[1], Chenhui Liu[1], Sicheng Li[1], Kun Cao[1], Yiping Yang[1], and Zhun Cheng[2,*]

[1]*Hunan University of Technology, Zhuzhou 412007, China*
[2]*Hunan Railway Professional Technology College, Zhuzhou 412001, China*

ABSTRACT: In order to solve the issues of large computation and control performance affected by motor parameters in the conventional model predictive torque control (MPTC) of permanent magnet synchronous motors (PMSMs), a robust model predictive torque control strategy with online parameter identification based on an improved differential evolution extended Kalman filter (IDEEKF-RMPTC) is proposed To begin with, and a steady-state voltage vector at the next time is obtained through a low-pass filter and used as the reference voltage vector to select the alternative voltage vector. The parameter robustness of the PMSM system is enhanced, and the computational effort is reduced. In addition, an improved differential evacuation algorithm for the extended Kalman filter (EKF) is designed, and the system noise matrix Q and measurement noise matrix R of the EKF are optimized. The estimation error is reduced; the stability of the system is enhanced; and the accuracy of the identification of the motor parameters is improved. Finally, the computational effort of the system is effectively reduced by the proposed IDEEKF-RMPTC strategy, and the parameter robustness of the PMSM drive system under parameter mismatch conditions is enhanced which are proved by the experimental results.

1. INTRODUCTION

PMSM is extensively applied in industrial production, aerospace and other fields because of its high efficiency, small size, and high power density [1]. The control methods primarily include field-oriented control (FOC) and direct torque control (DTC) [2]. FOC selects voltage vectors based on the torque and magnetic chain errors through a pre-given switching table, which is a simple control method but has limited optional voltage vectors, resulting in large torque and magnetic chain pulsations [3]. To solve the problem of large magnetic chain and torque pulsation in DTC, scholars have tried to introduce model predictive control (MPC) into DTC and achieved some success. MPC is generally used in power electronics and can be categorized into continuous control set MPC (CCS-MPC) and finite control set MPC (FCS-MPC) [4]. In a PMSM drive system, FCS-MPC methods can be categorized into model predictive current control (MPCC) and MPTC according to different control objectives [5].

MPTC suffers from the problems of large computation of torque pulsation in the prediction process, and control performance is strongly dependent on the model parameters. When real parameters are affected by temperature rise, magnetic field saturation, and other factors, the torque and magnetic chain prediction will produce errors, which deteriorate the control performance [6, 7]. To address the above problems, scholars have done much research and proposed various solutions.

To address the problem of large MPTC calculations and high torque and magnet flux linkage pulsations, scholars have done the following researches. In [8], an advanced deadband direct torque and flux control (ADB-DTFC) system is proposed. This strategy automatically adjusts phase and duration of the voltage vector to reduce torque fluctuation and stator flux ripple by determining the magnitude of the error between the torque and its reference value. But it requires a large computational cost for this method. In [9], a model-predictive dual-target current control (MPTCC) scheme based on the model-predictive control concept is proposed. First, a basic MPCC strategy is proposed for dealing with torque generation problem of the base member. Then, a modified cost function is proposed to provide a more accurate torque generation voltage vector. This strategy eliminates torque pulsations and reduces total harmonic distortion (THD), but with some delay. In [10], a novel fast response MPTC strategy for PMSM drives is proposed. The strategy converts the reference torque to the magnetic chain in the dq-axis, which reduces the computational effort of the system. But it is highly dependent on the accuracy of the motor parameters.

Aiming at the problem that motor performance of control is dependent on the accuracy of model parameters, scholars have done the following studies. In [11], a preliminary online parameter identification algorithm for PMSM deadband control (DBC) is proposed. The method establishes a well-recognized model to estimate the parameter error of the DBC offset to reduce the system's dependence on parameters. But the model needs to be continuously adjusted for complex and variable situations. In [12], a parametric identification method using a

* Corresponding author: Zhun Cheng (120277982@qq.com).

high-frequency (HF) equivalent impedance model of PMSM is proposed. The method identifies resistance and *dq*-axis inductance offline and online, and identifies magnetic flux linkage online. In [13], a disturbance feedforward compensation-based-model predictive torque control (DFCB-MPTC) of induction machine is proposed to compensate the lumped disturbances and enhance the parameter robustness of the system. But it requires more computational cost. In [14], a robust model predictive voltage control (MPVC) scheme is proposed to improve the parametric robustness of MPVC for SPMSM drivers. But it is difficult to debug and design. In [15], a current prediction error model considering the uncertainty of model parameters is proposed to effectively reduce the current harmonic content, current fluctuation, and current tracking error due to parameter mismatch. But this model model design is complex and computationally intensive.

Scholars have carried out the following studies from the perspective of EKF to address the issue that motor control performance is dependent on the accuracy of the model parameters. In [16], two Kalman filter (KF) based online recognition solutions are proposed. One scheme consists of an extended KF, and the other scheme uses a double extended KF. Both the schemes are applicable to any identifiable combination of electrical parameters, but the computational complexity is higher. In [17], an extended Kalman filter (EKF)-based inductance estimation strategy for single-phase open DTP-PMSMs is proposed to improve the control performance of DTP-PMSMs under open-phase faults. But because the Q and R of the EKF are constant values, it recognizes the parameters inaccurately. In [18], a noninvasive online method is proposed. The approach uses Vold-KF order tracking (VKF-OT) and dynamic Bayesian network (DBN) to detect the rotor demagnetization in real time. The electromagnetic interference of the torque is eliminated. Uniform demagnetization is detected in wide range of motor speed. But the method requires training and optimization of a large amount of experimental data. In [19], a robust DPCC (RDPCC) is proposed. It uses KF based on extended state modeling (ESM) to estimate states and disturbances. Although the KF can reduce disturbances in prediction and disturbances caused by changes in estimated parameters, it still produces some delay effects. In [20], a scheme for the fusion of electrical model-based estimation and mechanical model-based observers is proposed. The strategy employs extended Kalman filter (EKF) to fuse the mechanical motion sensing and estimation information, and introduces a disturbance suppressor to counteract the parameter imprecision and inconstancy of the EKF model. But this method occupies large computational resources of the system. In [21], a method for filtering measurement noise using EKF and adaptive linear active disturbance rejection control (LADRC) strategies is proposed, but it requires a large computational cost.

To address the problem that MPTC calculation and torque pulsation are large in PMSM drive systems and the control performance is affected by motor parameters, a novel IDEEKF-RMPTC strategy is proposed. Compared to the conventional MPTC, this method has better parameter robustness and less computation of the system, and the major contributions of this paper are as follows:

1) The RMPTC strategy utilizes feature that actual voltage vector position is fixed during the steady state operation of the motor to select alternative voltage vectors based on the steady state voltage vector, which reduces system computation and enhances the parameter robustness of the PMSM.

2) The IDEEKF strategy replaces the original fixed-invariant mutation strategy of differential evolutionary (DE) with four test vector generation strategies, which allows the Q and R of the EKF to be adaptively adjusted according to the changes of motor parameters. It improves the recognition accuracy of EKF and enhances the parameter robustness of PMSM

The rest of this paper is as follows. Section 2 introduces the mathematical model of the PMSM. Section 3 introduces the basic principle of conventional MPTC and EKF. Section 4 introduces The basic principle of IDEEK-RMPTC. Sections 5 show The experimental validation and simulation analysis. Finally, Section 6 briefly summarizes this paper.

2. MATHEMATICAL MODEL OF PMSM

In this paper, the surface-mounted PMSM is studied, and the voltage and magnet flux linkage equations in the two-phase rotating *dq* coordinates system are as follows:

$$\begin{cases} u_d = R_s i_d + \frac{d\psi_d}{dt} - \omega_e \psi_q \\ u_q = R_s i_q + \frac{d\psi_q}{dt} + \omega_e \psi_d \end{cases} \tag{1}$$

$$\begin{cases} \psi_d = L_s i_d + \psi_f \\ \psi_q = L_s i_q \end{cases} \tag{2}$$

The electromagnetic torque equation is as follows:

$$T_e = \frac{3}{2} p \psi_f i_q \tag{3}$$

where u_d, u_q are the *dq*-axis components of stator voltage vector; i_d, i_q are the *dq*-axis components of stator current vector; ψ_d, ψ_q, and ψ_f are the *dq*-axis components of the stator and the rotor magnetic flux linkage vector; R_s and L_s are stator resistance and stator inductance; and ω_e is the rotor angular velocity of the motor

Using the first-order Eulerian discretization method to discretize (1), the resulting current prediction model is as follows:

$$\begin{cases} i_d(k+1) = i_d(k) + \frac{T_s}{L_s}[u_d(k) - R_s i_d(k) + L_s \omega_e i_q(k)] \\ i_q(k+1) = i_q(k) + \frac{T_s}{L_s}[u_q(k) - R_s i_q(k) - L_s \omega_e i_d(k) - \omega_e \psi_f] \end{cases} \tag{4}$$

where k represents the sampling value at current moment, and $k+1$ represents the sampling value at next time. T_s is the value of the sampling period.

3. THE BASIC PRINCIPLE OF CONVENTIONAL MPTC AND EKF

3.1. The Principle of MPTC

The main steps of the conventional MPTC (CMPTC) include the division of voltage vectors, the design of the cost function, and the optimal voltage vector selection.

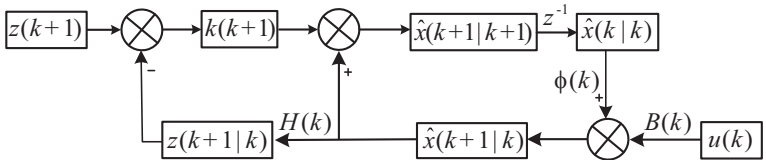

FIGURE 1. The schematic diagram of EKF.

1) The division of voltage vectors

A three-phase two-level voltage source type inverter has eight switching states, i.e., six non-zero voltage vectors and two zero vectors.

2) The design of cost functions

The MPTC mainly uses torque and magnet flux linkage as the control objectives, and the formula is as follows:

$$g = \left|T_e^{ref} - T_e(k+1)\right| + \lambda \left|\psi_s^{ref} - |\psi_s(k+1)|\right| \quad (5)$$

where λ is the weighting factor usually established through empirical methods.

3) The optimal voltage vector selection

Firstly, bring seven basic voltage vectors into the current prediction model (4) to derive the predicted value of current after one T_s for each basic voltage vector, and derive predicted values of torque and magnetic chain from this predicted value. Secondly, the predicted values are substituted into cost function and voltage vector with the smallest cost function selected as the optimal voltage vector. Finally, apply the switching state corresponding to optimal voltage vector to the inverter to generate the superimposed three-phase currents to control the motor.

The MPTC needs to traverse seven optimization searches, which is computationally intensive, and the control performance of the motor is strongly dependent on the motor parameters. Therefore, in this paper, the RMPTC strategy is proposed to reduce the computational effort and enhance the robustness of the system parameters.

3.2. The Basic Principle of Parameter Identification Based on EKF Algorithm

The EKF algorithm is an optimal recursive estimation algorithm for nonlinear systems. In the parameter identification of PMSM, the motor parameters that vary with the running time are considered as part of the extension, and these motor parameters are estimated through the filtering process for identification purposes [22].

The nonlinear system yields a linear model expression as follows:

$$\begin{cases} x(k+1) = \phi(k)x(k) + B(k)u(k) + w(k) \\ z(k) = H(k)x(k) + v(k) \end{cases} \quad (6)$$

where $x(k)$ is the state vector of the system; $u(k)$ is the input vector of the system; $z(k)$ is the observation vector of the system; $w(k)$ is the process noise; $v(k)$ is the observation noise; k is the current iteration number; $B(k)$ is the control input matrix; $H(k)$ is the state observation matrix; $\varphi(k)$ is the state transfer matrix. $w(k)$ and $v(k)$ are white noises with mean value, and their expectation values satisfy $E\{W(k)\} = 0$, $E\{V(k)\} = 0$.

In the online identification of motor parameters by using EKF, there are two parameters particularly important. The first one is the process noise covariance matrix Q, which represents uncertain random noise generated in dynamics of the motor drive system. The other is the measurement noise covariance matrix R, which represents the random noise caused by measurement errors in the measurement process. Either large or small Q and R will cause the parameter estimation error and the control performance of the motor to deteriorate.

In the EKF $Q = E\{WW^T\}$, $R = E\{VV^T\}$. W and V represent the noise vectors. The EKF schematic is shown in Fig. 1. It consists of two steps: prediction and update.

The PMSM is a fifth-order nonlinear strongly coupled system, so in this paper, the reduced-order parallel dual EKFs are used to recognize the parameters of the PMSM in order to reduce the coupling of motor parameters and improve parameter identification ability.

Firstly, the value of R_s is observed by the EKF observer, and then its value is used to recognize the magnetic flux linkage and inductance [23]. The recognition equations are as follows:

$$\frac{d}{dt}\begin{bmatrix} i_{d1} \\ i_{q1} \\ \psi_f \\ L_s \end{bmatrix} = \begin{bmatrix} -\frac{R_s}{L_s} & \omega_e & 0 & 0 \\ -\omega_e & -\frac{R_s}{L_s} & 0 & 0 \\ 0 & 0 & 0 & 0 \\ 0 & 0 & 0 & 0 \end{bmatrix} \begin{bmatrix} i_{d1} \\ i_{q1} \\ \psi_f \\ L_s \end{bmatrix} + \begin{bmatrix} \frac{1}{L_s} & 0 \\ 0 & \frac{1}{L_s} \\ 0 & 0 \\ 0 & 0 \end{bmatrix} \begin{bmatrix} u_d \\ u_q \end{bmatrix} + \begin{bmatrix} 0 \\ -\frac{\omega_e \psi_f}{L_s} \\ 0 \\ 0 \end{bmatrix} \quad (7)$$

The Eulerian discretization of (7) yields the following Jacobi matrices ϕ_1 for the magnetic chain and inductance as follows:

$$\phi_1 = I + \frac{\partial f(x_1)}{\partial x_1}\bigg| x_1 = \hat{x}_1(k)$$

$$= \begin{bmatrix} 1 - LR_sT_s & \omega_e T_s & 0 & -R_s i_{d1} T_s \\ -\omega_e T_s & 1 - LR_sT_s & -L\omega_e T_s & -(R_s i_{q1} + \omega_e \psi_f) T_s \\ 0 & 0 & 1 & 0 \\ 0 & 0 & 0 & 1 \end{bmatrix} \quad (8)$$

where $x_1 = [i_{d1}, i_{q1}, \psi_f, L_s]^T$ is the state-variable matrix of the chains and inductors, and L is the inverse of the inductor L_s.

The measurement equations are shown as follows:

$$z_1 = \begin{bmatrix} 1 & 0 & 0 & 0 \\ 0 & 1 & 0 & 0 \end{bmatrix} \begin{bmatrix} i_{d1} & i_{q1} & \psi_f & L_s \end{bmatrix}^T \quad (9)$$

Equally, the identified magnetic chain and inductance are used as fixed values to identify the resistance, and the identified expression is as follows:

$$\frac{d}{dt}\begin{bmatrix} i_{d2} \\ i_{q2} \\ R_s \end{bmatrix} = \begin{bmatrix} -LR_s & \omega_e & 0 \\ -\omega_e & -LR_s & 0 \\ 0 & 0 & 0 \end{bmatrix}\begin{bmatrix} i_{d2} \\ i_{q2} \\ R_s \end{bmatrix} + \begin{bmatrix} L & 0 \\ 0 & L \\ 0 & 0 \end{bmatrix}\begin{bmatrix} u_d \\ u_q \end{bmatrix} + \begin{bmatrix} 0 \\ -\omega_e\psi_f L \end{bmatrix} \quad (10)$$

By discretizing (10) according to the antecedent Euler, one obtains the Jacobian of the resistance ratio ϕ_2 as follows:

$$\begin{aligned} \phi_2 &= I + \frac{\partial f(x_2)T_s}{\partial x_2}|x_2 = \hat{x}_2(k) \\ &= \begin{bmatrix} 1 - LR_sT_s & \omega_eT_s & -Li_{d2}T_s \\ -\omega_eT_s & 1 - LR_sT_s & -Li_{q2}T \\ 0 & 0 & 1 \end{bmatrix} \end{aligned} \quad (11)$$

where $x_2 = [i_{d2}, i_{q2}, R_s]^T$ is the state variable matrix of the recognized resistance.

The measurement equations are shown as follows:

$$z_2 = \begin{bmatrix} 1 & 0 & 0 \\ 0 & 1 & 0 \end{bmatrix}\begin{bmatrix} i_{d2} & i_{q2} & R_s \end{bmatrix}^T \quad (12)$$

The EKF-based PMSM parameter identification deals with the nonlinearity of the motor by linearizing its nonlinear model, which is able to adapt to the variation of the motor drive system parameters in order to achieve its online identification function. Since the EKF combines state and parameter estimation and utilizes filtering for parameter estimation, it is particularly important to obtain the matrix R of the filter and the matrix Q of the system. In this paper, IDEEKF is introduced to correct the Q and R of the system, which reduces filtering errors and prediction delays and improves the recognition accuracy of the EKF.

4. THE BASIC PRINCIPLE OF IDEEKF-RMPTC

4.1. The Design of Robust Model Predictive Torque Control

The conventional MPTC uses the parameters of the motor when calculating the reference voltage vector and predicting the current value at the next moment. When the motor parameters are inaccurate, the problems of inaccurate prediction model and deteriorated control performance occur. To address this problem, an RMPTC strategy is proposed.

Since there is a delay in predictive control of PMSM, the optimal vector selected in the MPTC cannot be applied to the PMSM until the next control cycle, which leads to poor system performance. In this paper, the effect of delay on the control performance of the system is eliminated by compensating the delay in the current. The prediction model of current value, magnetic chain value, and torque value at $(k+2)$ is as follows:

$$\begin{cases} \psi_d(k+2) = \psi_d(k+1) + T_s\left[u_d(k+1) - R_s i_d(k+1) + \omega_e\psi_q(k+1)\right] \\ \psi_q(k+2) = \psi_q(k+1) + T_s\left[u_q(k+1) - R_s i_q(k+1) - \omega_e\psi_d(k+1)\right] \\ i_q(k+2) = i_q(k+1) + \frac{T_s}{L_s}\left[u_q(k+1) - i_q(k+1)R_s - L_s\omega_e i_d(k+1) - \omega_e\psi_f\right] \\ T_e(k+2) = \frac{3}{2}p\psi_f i_q(k+2) \end{cases} \quad (13)$$

According to the deadbeat control of torque and magnetic flux linkage, the expression for the reference voltage vector is derived as follows:

$$\begin{cases} u_d^{ref} = u_d(k+1) = \frac{1}{T_s}[\psi_d(k+2) - \psi_d(k+1) + T_sR_si_d(k+1) - T_s\omega_e\psi_q(k+1)] \\ u_q^{ref} = u_q(k+1) = \frac{1}{T_s}[\psi_q(k+2) - \psi_q(k+1) + T_sR_si_q(k+1) + T_s\omega_e\psi_d(k+1)] \end{cases} \quad (14)$$

Transforming (14) to the equations in the two-phase stationary $\alpha\beta$ coordinate system is as follows:

$$\begin{bmatrix} u_\alpha^{ref} \\ u_\beta^{ref} \end{bmatrix} = \begin{bmatrix} \cos\theta_e & -\sin\theta_e \\ \sin\theta_e & \cos\theta_e \end{bmatrix}\begin{bmatrix} u_d^{ref} \\ u_q^{ref} \end{bmatrix} \quad (15)$$

where θ_e represents the angle between d-axis and α-axis.

TABLE 1. The table of alternative voltage vector.

Sector number	Reference Voltage Vector Ang θ_s	Alternative Voltage Vector
1	$(0, \pi/3]$	$u_1, u_2, u_0(u_7)$
2	$(\pi/3, 2\pi/3]$	$u_2, u_3, u_0(u_7)$
3	$(2\pi/3, \pi]$	$u_3, u_4, u_0(u_7)$
4	$(\pi, 4\pi/3]$	$u_4, u_5, u_0(u_7)$
5	$(4\pi/3, 5\pi/3]$	$u_5, u_6, u_0(u_7)$
6	$(5\pi/3, 2\pi]$	$u_6, u_1, u_0(u_7)$

The alternative voltage vector table is shown in Table 1, in which θ_s is the angle between the reference voltage vector u^{ref} and the α-axis. The expression is as follows:

$$\theta_s = \begin{cases} \arccos\left(\frac{u_\alpha^{ref}}{u^{ref}}\right) & u_\beta^{ref} \geq 0 \\ -\arccos\left(\frac{u_\alpha^{ref}}{u^{ref}}\right) + 2\pi & u_\beta^{ref} < 0 \\ u^{ref} = \sqrt{(u_\alpha^{ref})^2 + (u_\beta^{ref})^2} \end{cases} \quad (16)$$

The voltage vector to be selected is then chosen by determining the range of θ_s in order to reduce the number of predictions made by the system, thus reducing the computational effort of the system.

By analyzing the reference voltage vector angle θ_s, it can be concluded that θ_s is closely related to the motor parameters of PMSM. When PMSM parameters are inaccurate, θ_s is calculated incorrectly; the optimal voltage vector is excluded; and

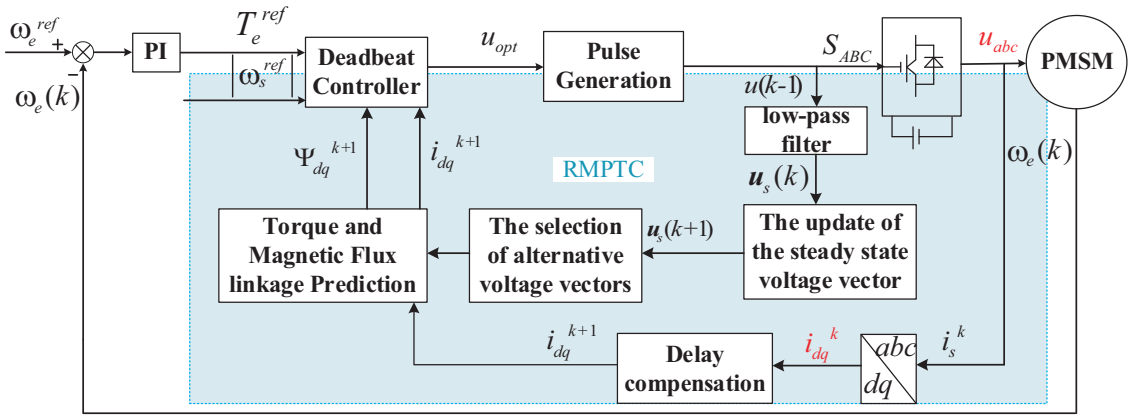

FIGURE 2. The control diagram of RMPTC strategy.

the system control performance is degraded. To address these existing problems, an MPTC control strategy with parameter robustness is proposed in this section.

When the motor runs to a steady state, state variables such as speed and stator current change slowly and can be considered as constants. Compared to one control cycle, the slow changes in motor parameters can be approximated as constant, and the corresponding steady state voltage vector is little affected by the changes in motor parameters. Using this feature, the RMPTC is designed, and the control block diagram of the system is shown in Fig. 2.

Since the signals generated by the inverter contain high-frequency switching signals, the high-frequency switching signals must be filtered out to obtain the low-frequency switching signals corresponding to the steady-state voltage vector. In this paper, by designing a low-pass filter, the voltage vector acting on each cycle is filtered through the low-pass filter to obtain the steady-state voltage vector corresponding to the low-frequency switching signal. The steady state voltage of the current cycle is as follows:

$$\begin{cases} \widehat{\mathbf{u}}_s(k) = \mathbf{u}_s(k-1)Q(s) \\ Q(s) = \frac{1}{1+\tau s} \end{cases} \tag{17}$$

where $\widehat{\mathbf{u}}_s(k)$ is the steady state voltage in the dq coordinate system at the current cycle, $\mathbf{u}_s(k-1)$ the voltage vector in the dq coordinate system that is applied to the motor at the $k-1$ cycle, $Q(s)$ the first-order low-pass filter, and τ the time constant, which is the inverse of the value of angular frequency.

Since there is a positional deviation between the steady-state voltage vector of the current cycle and the steady-state voltage vector of the next cycle, the steady-state voltage vector is corrected for the positional deviation after it is obtained through the filter. The expression of the corrected steady state voltage vector is as follows:

$$\widehat{\mathbf{u}}_s(k+1) = \widehat{\mathbf{u}}_s(k)e^{j\omega_e T_s} \tag{18}$$

After obtaining the reference voltage vector for the next cycle, the candidate voltage vectors are selected by Table 1 to reduce the number of predictions of the system and to enhance the robustness of the parameters of the system during steady state operation.

The strategy for selecting alternative voltage vectors based on steady-state voltage vectors is as follows:

1) If the optimal voltage vector selected in the previous cycle is a zero vector, the alternative voltage vectors are all the fundamental voltage vectors.

2) If a connected zero vector is selected for two consecutive cycles, the alternative voltage vectors are that vector and the effective electric vectors neighboring that vector.

3) In the remaining cases, the alternative vectors are selected according to Table 1.

The proposed RMPTC strategy is designed to select an alternative voltage vector table based on the steady state voltage vector in this paper by utilizing the characteristic of the actual voltage vector position being fixed and unchanged during the steady state operation of the motor. The optimal voltage vector that was originally excluded from the alternative voltage vector group due to parameter mismatch is reincluded in the candidate voltage vector table, allowing the optimal voltage vector to be selected as the output voltage vector one or two cycles after the parameter mismatch. This improves the control performance of the system and reduces the computational effort.

4.2. The Design of Improved Differential Evolution EKF

Since the PMSM drive system is highly dependent on the motor parameters, the ability of RMPTC to enhance the robustness of the motor parameters is limited. Therefore, we enhance the parameter robustness of the system from the point of view of recognizing the motor parameters by EKF, whereas Q and R in EKF are fixed values with nonuniform setting standard, and repeated experiments and adjustments are required to obtain the correct values. The intelligent algorithm can realize the dynamic adjustment of Q and R.

There are many algorithms to improve the Q and R of EKF, such as Genetic Algorithm (GA), Particle Swarm Algorithm (PSO), and Differential Evolutionary Algorithm (DE). GA requires larger population size and more iterations, and have slower convergence speed. PSO is more sensitive to the initial parameter selection and may stall near the local optimal so-

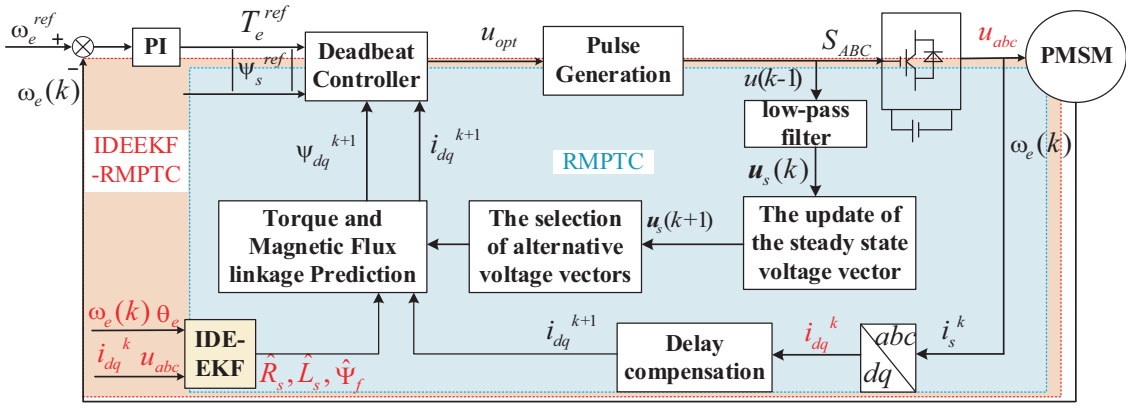

FIGURE 3. The control diagram of IDEEKF-RMPTC strategy.

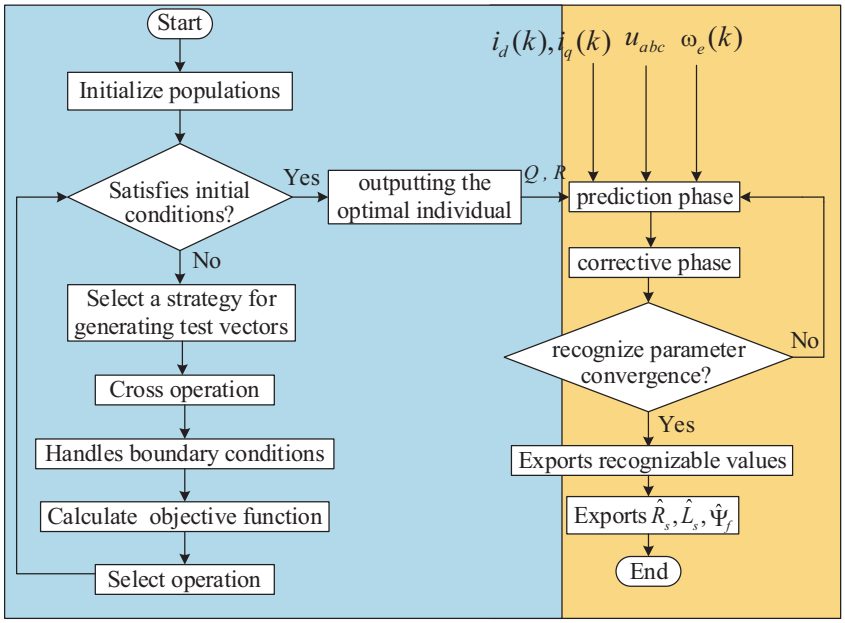

FIGURE 4. The flowchart of IDEEKF.

lution. DE has the advantages of simplicity, ease of use, few parameters, and fast convergence speed, but it lacks flexible parameter adjustment and adaptive mechanism, which makes it less adaptive and robust [24].

The IDE algorithm designed in this paper replaces the original fixed and unchanging mutation strategy of DE with four test vector generation strategies, which has the ability of dynamically adjusting the mutation factor and crossover probability, and can optimize Q and R more efficiently under different mutation conditions, thus improving the ability of EKF to identify the parameters and enhancing the robustness of the system parameters.

The control diagram for the IDEEKF-RMPTC strategy is shown in Fig. 3 where IDEEKF inputs are the operating parameters such as current and voltage of the motor, and the outputs are the real-time estimates of the motor parameters. This module is able to identify the motor parameters accurately in time, thus making the prediction model more accurate and improving the control performance of the system.

The flowchart of IDEEKF operation is shown in Fig. 4, which consists of two parts: the IDE optimizes the Q and R of the EKF and recognizes the motor parameters online by the EKF. When the EKF obtains the optimized Q and R from the IDE, the error and time for the EKF to identify the motor parameters are reduced. The parameter robustness of the system is enhanced.

The IDE algorithm is designed to replace the original fixed mutation strategy of the DE algorithm with four test vector generation strategies. The experience of learning the optimal solution in the previous generation through experimental vector generation strategies leads to adaptive and more appropriate

generation strategies. The equation for the strategy for generating the four test vectors is as follows:

1) The $DE/rand/1/bin$ policy. Its equation is as follows:

$$U_i^j = \begin{cases} X_{r_1}^j + F(X_{r_2}^j - X_{r_3}^j), & rand[0,1) < CR \ or \ j = j_{rand} \\ X_i^j, & otherwise \end{cases} \quad (19)$$

2) The $DE/rand\text{-}to\text{-}best/2/bin$ policy. Its equation is as follows:

$$U_i^j = \begin{cases} X_{r_1}^j + F(X_{best}^j - X_i^j) + F(X_{r_1}^j - X_{r_2}^j) + \\ F(X_{r_3}^j - X_{r_4}^j), \ if rand\,[0,1) < CR \ or \ j = j_{rand} \\ X_i^j, \ otherwise \end{cases} \quad (20)$$

3) The $DE/rand/2/bin$ policy. Its equation is as follows:

$$U_i^j = \begin{cases} X_{r_1}^j + F(X_{r_2}^j - X_{r_3}^j) + F(X_{r_4}^j - X_{r_5}^j), \\ \quad if rand\,[0,1) < CR \ or \ j = j_{rand} \\ X_i^j, \ otherwise \end{cases} \quad (21)$$

4) The $DE/current\text{-}to\text{-}rand/1$ policy. Its equation is as follows:

$$U_{i,G} = X_{i,G} + K(X_{r_1,G} - X_{i,G}) + F(X_{r_2,G} - X_{r_3,G}) \quad (22)$$

where U_i^j is the new individual produced by the mutation operation, $X_i^j (i = r_1, r_2, \ldots)$ a randomly selected individual in the population, F the mutation operator, CR the crossover operator. F is used to introduce randomness in each generation to maintain the diversity of populations and to find new solutions in the search space. CR is used to generate new offspring individuals by combining the characteristics of different individuals. i is the sequence of the individual in the population, D the vector dimensionality, and $j = \{1, 2, \ldots, D\}K$ a random number between $(0, 1)$.

The IDE algorithm is designed to find out the optimal individuals (the optimal individuals are the optimal Q and R) in the population by iteratively initializing the population, evaluating the fitness, performing mutation and crossover operations, and selecting the good individuals. The specific steps are as follows:

1) The initialized strategy probabilities $P_{n,G}$ and LP, and a set of populations with NP of 50 are randomly generated with initial population formulas as follows:

$$\begin{cases} X_{i,G}^j = x_{\min}^j + rand(0,1)(X_{\max}^j - X_{\min}^j) \\ X_{i,G} = \left\{ X_{i,G}^1, \ X_{i,G}^2, X_{i,G}^3, \ldots, X_{i,G}^D \right\} \\ X_{\min} = \left\{ x_{\min}^1, x_{\min}^2, x_{\min}^3, \ldots, x_{\min}^D \right\} \\ X_{\max} = \left\{ x_{\max}^1, x_{\max}^2, x_{\max}^3, \ldots, x_{\max}^D \right\} \\ i = \{1, 2, 3, \ldots, NP\} \end{cases} \quad (23)$$

where D is the vector dimension.

2) The boundedness handling process: new individuals that do not meet the boundary constraints are reinitialized in the search space.

3) The strategy selection: randomly select a strategy for each target vector $X_{i,G}$ and compute the strategy probability $P_{n,G}$ and update the success and failure memories.

4) The variation and crossover operation: a variation operation is performed on the experimental vector generation strategy with the highest strategy after boundary processing [25]. The expression for the crossover operation is as follows:

$$H_{i,G+1} = \begin{cases} U_{i,G+1}, & if rand(j) \le CR \\ X_{i,G}, & otherwise \end{cases} \quad (24)$$

$$f = w_1 e_1 + w_2 e_2 \quad (25)$$

$$e = (i_E - i)^2 \quad (26)$$

where w_1 and w_2 are the weights of the corresponding state variables of Q and R, and e is the error term of the dq-axis current observation i_E and the EKF estimate i. e_1 corresponds to the error of the d-axis current, and e_2 corresponds to the error of the q-axis current.

5) The selection operation: bring the individual $X_{i,G+1}$ of the new population and the individual $X_{i,G}$ of the previous generation population into (25) for size comparison, and select the one with the highest value of f as the new individual of the current population. If the current population has evolved to the maximum number of iterations, the new individual of the current population is output as the optimal solution, and if not, the mutation operation is continued. The expression for the selection operation is as follows:

$$Xi, G+1 = \begin{cases} U_{i,G+1}, & f(U_{i,G+1}) < f(X_{i,G}) \\ X_{i,G}, & otherwise \end{cases} \quad (27)$$

The proposed IDE algorithm can be used to optimize the Q and R of EKF. It takes Q and R as the variables of the optimization problem and dynamically adjusts Q and R through operations such as population evolution, selection, crossover, and mutation. It makes the EKF obtain better filtering effect in the process of parameter estimation and state estimation. The estimation error and time of EKF are reduced. When parameter mismatch occurs, the system can obtain more accurate motor parameters, which leads to improved parameter robustness.

5. EXPERIMENTAL RESULTS AND ANALYSIS

To verify the correctness and effectiveness of the proposed method IDEEKF-RMPTC, simulation experiments are carried out on an RT-LAB semi-physical simulation platform based on a TMS320F2812 controller, comparing the schemes of EKF-RMPTC and EKF-MPTC. The model is first downloaded to the simulation platform to realize the building of the hardware-in-the-loop system of the PMSM drive system, and then the Oscilloscope DPO 4034 to show the experimental results. The RT-LAB semi-physical simulation platform is shown in Fig. 5(a), The schematic diagram of the RT-LAB hardware in the loop is shown in Fig. 5(b), and the parameters of PMSM are shown in Table 2.

Because the parameters cannot be set arbitrarily when the PMSM is running, in this experiment, the parameters of the motor under parameter mismatch are replaced by setting the corresponding step change module. The working conditions are set as follows: the rotational speed is 750 r/min; the motor

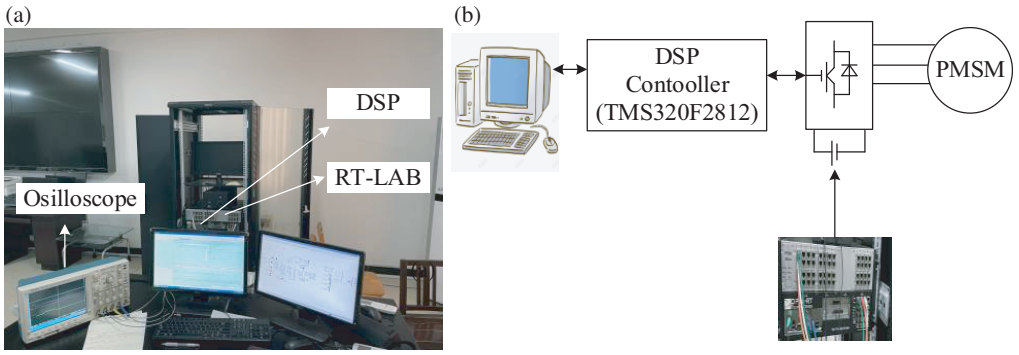

FIGURE 5. (a) The diagram of RT-LAB semi-physical simulation platform. (b) The schematic diagram of the RT-LAB hardware.

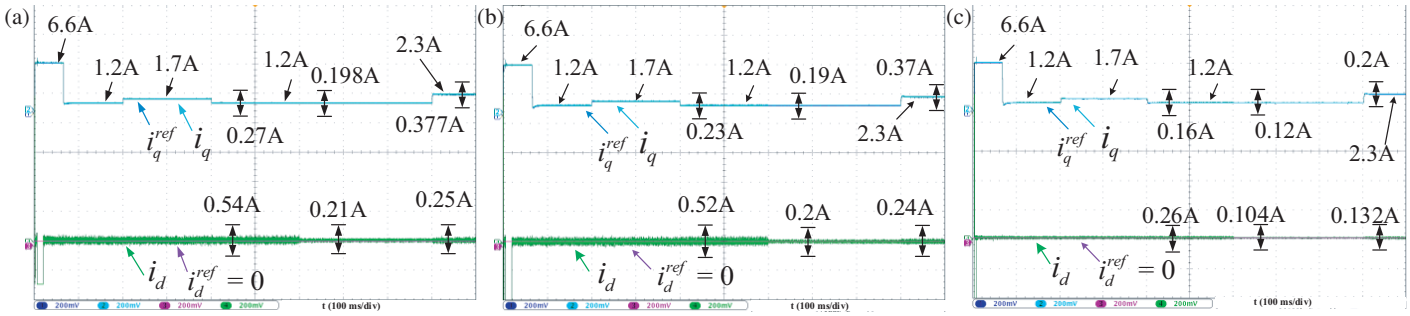

FIGURE 6. The waveforms of *dq*-axis current. (a) EKF-MPTC. (b) EKF-RMPTC. (c) IDEEKF-RMPTC.

TABLE 2. The parameters of PMSM system.

Parameter	Symbol	Value
Number of pole pairs	n_p	4
Stator inductance	L_s	8.5 mH
Stator resistance	R_s	2.875 Ω
Magnet flux linkage	ψ_f	0.3 Wb
DC voltage	U_{dc}	380 V
Rated torque	T_e	12 N · m
Rated speed	N	750/min
Rated power	P_N	1 kW
Inertia	J	0.00816 kg · m^2

is started with load, 0.2 s loading operation, 0.4 s load reduction operation, 0.6 s inductance mismatch (IM), 0.8 s resistance mismatch, and 0.9 s magnetic flux linkage mismatch (MFLM).

This experiment is organized as follows:

1) The parameter robustness of MPTC and RMPTC under parameter mismatch is verified by comparing EKF-MPTC with EKF-RMPTC, and the experimental results show that RMPTC is more parameter robust under the same experimental conditions.

2) Compare EKF-RMPTC with IDEEKF-RMPTC to verify the ability of IDEEKF and EKF to recognize the motor parameters under parameter mismatch, and the experimental results show that IDEEKF is more capable of recognizing the parameters under parameter mismatch.

5.1. The Dynamic Working Condition Analysis of dq-Axis Current

A waveform of the *dq*-axis current under the three control strategies is shown in Fig. 6. It can be seen that the dynamic tracking ability of the *dq*-axis current is basically the same under the three sets of experiments. With 0.6 s as the dividing line, it is divided into no parameter mismatch and parameter mismatch. By parameter identification the motor parameters are recognized in real time and returned to the control strategy to participate the calculation. During stable operation of the motor, the *dq*-axis current amplitudes of the three methods are different. By observing Figs. 6(a)-(b) and Table 3, it is seen that the *dq*-axis current amplitude gets reduced in RMPTC compared to MPTC when parametric mismatch occurs between the inductance and stator magnet flux linkage. By comparing Fig. 6(b) and Fig. 6(c), it can be seen that IDEEKF significantly improves the accuracy of motor identification compared to EKF, which leads to a significant reduction in the amplitude of the *dq*-axis currents, indicating that IDEEKF is more robust in parameters identification.

TABLE 3. The *dq* axis current amplitude.

The control of strategy	The amplitude of the d-axis current	The amplitude of the q-axis current
EKF-MPTC	0.54 A	0.27 A
EKF-RMPTC	0.52 A	0.23 A
IDEEKF-RMPTC	0.26 A	0.16 A

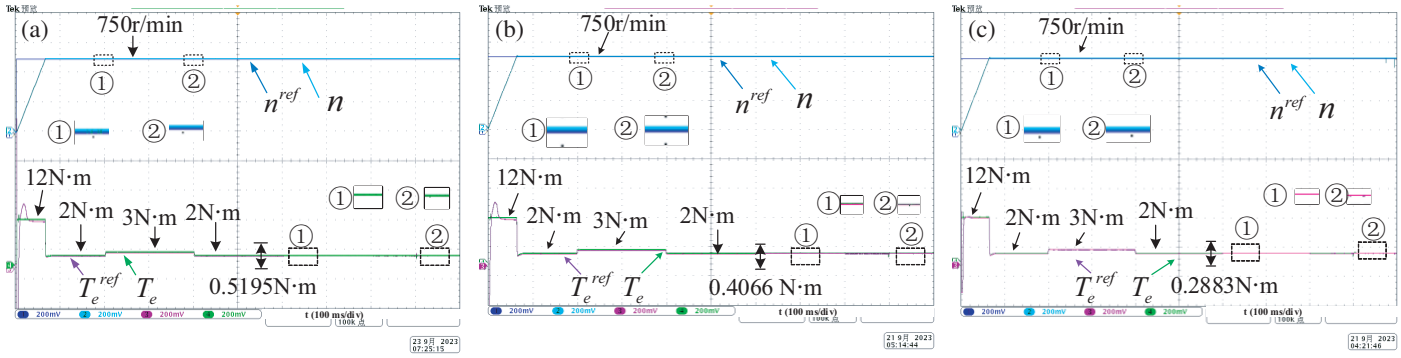

FIGURE 7. The waveforms of speed and torque. (a) EKF-MPTC. (b) EKF-RMPTC. (c) IDEEKF-RMPTC.

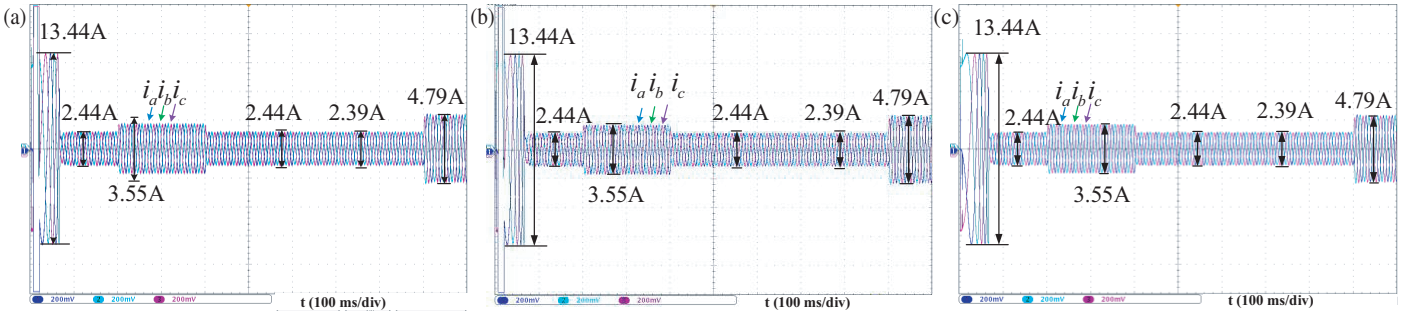

FIGURE 8. The waveform of ABC three-phase current. (a) EKF-MPTC. (b) EKF-RMPTC. (c) IDEEKF-RMPTC.

5.2. The Dynamic Working Condition Analysis of Speed and Torque

The speed and torque waveforms under the three control strategies are shown in Fig. 7. Because of the limited display scale of the oscilloscope, the overshoot of the rotational speed in Fig. 7 is not obvious, and the overshoot can be observed after several zooms in the actual operation. It can be observed that the dynamic following of the speed and torque waveforms under the three strategies are basically similar. By observing Figs. 7(a)-(b) and Table 4, the torque pulsation is reduced in RMPTC compared to MPTC when parameter mismatch occurs, indicating that IMPTC has better restraining of torque fluctuation.

TABLE 4. The result of speed response time and torque pulsation value.

The control of strategy	Speed respone time (ms)	torque pulsation value (N·m)
EKF-MPTC	66.67	0.5195
EKF-RMPTC	64.2	0.4066
IDEEKF-RMPTC	63.31	0.2883

5.3. The Stator Current and Its Harmonic Analysis

The ABC three-phase current waveform is shown in Fig. 8, and a-phase stator current waveform with FFT analysis is shown in Fig. 9. By comparing Fig. 8(b) and Fig. 8(c), the proposed strategy IDEEKF-RMPTC is concluded to have better stator current waveform. By comparing Fig. 9(b) and Fig. 9(c), the proposed strategy IDEEKFRMPTC is concluded to have smaller stator current harmonics. The THD value of EKF-MPTC is 4.06%; the THD value of EKF-RMPTC is 3.45%; and the THD value of IDEEKF-RMPTC is 2.49%. Compared to the EKF-RMPTC, the current harmonics of the IDEEKF-RMPTC are reduced by 27.82%. Compared to the EKF-MPTC, the current harmonics of the IDEEKF-RMPTC are reduced by 38.76%.

5.4. The Analysis of the Identification Results of the PMSM Parameters

Figure 10 shows the result of the identification of R_s. By observation, it can be seen that the resistance changes from R_s to $0.5R_s$ in 0.8 s. Based on Table 5, it can be seen that the pro-

TABLE 5. The result of parameter identification under two strategies.

Parameter	EKF		IDEEKF	
	Before mismatch	After mismatch	Before mismatch	After mismatch
R_s/Ω	2.9435	1.5196	2.9161	1.4889
Error/%	2.3826	5.7113	1.4296	3.7496
Recognition time/s	0.0249	0.0248	0.0068	0.0065
L_s/mH	7.9308	17.3795	8.1205	17.3036
Error/%	6.6961	2.2321	4.4647	1.7859
Recognition time/s	0.0265	0.0320	0.0053	0.0046
ψ_f/ Wb	0.2894	0.1453	0.3047	0.1461
Error/%	3.5333	2.3133	1.5667	2.6000
Recognition time/s	0.0652	0.0051	0.0041	0.0035

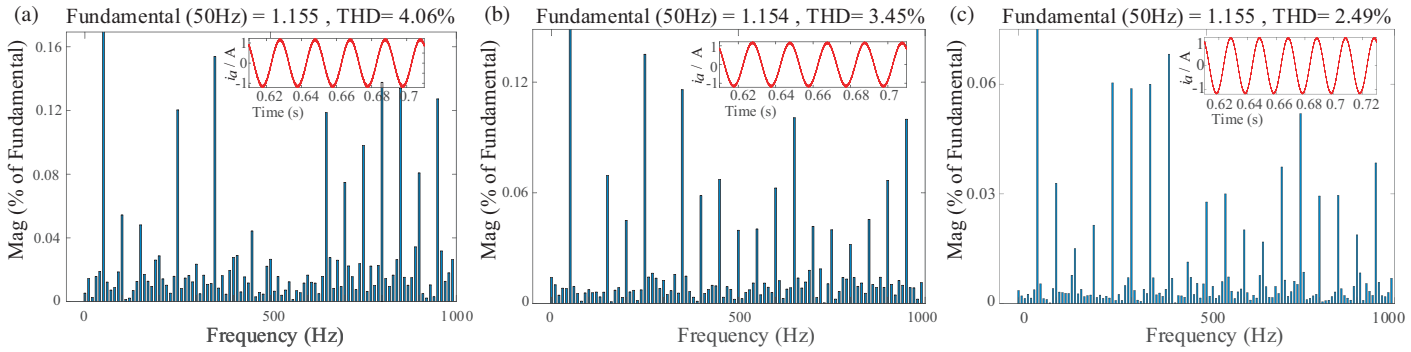

FIGURE 9. The diagram of phase current and its FFT analysis. (a) EKF-MPTC. (b) EKF-RMPTC. (c) IDEEKF-RMPTC.

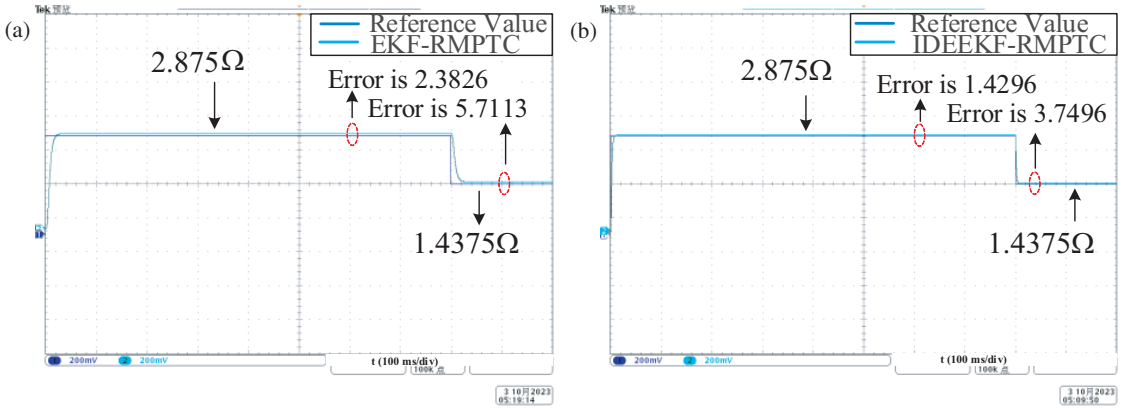

FIGURE 10. The identification result diagram of R_s. (a) EKF-RMPTC. (b) IDEEKF-RMPTC.

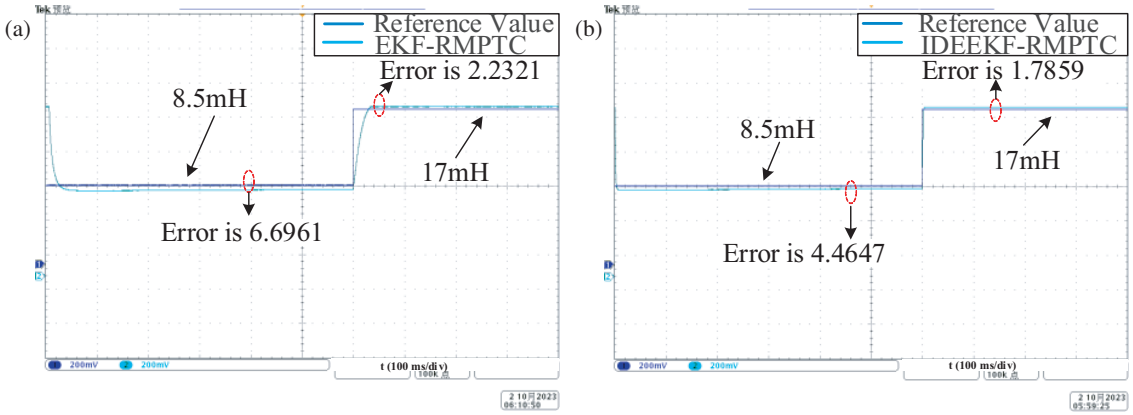

FIGURE 11. The identification result diagram of *Ls*. (a) EKF-RMPTC. (b) IDEEKF-RMPTC.

posed method IDEEKF-RMPTC has a recognized R_s value of 2.9161 Ω in 0 ∼ 0.8 s, with the recognition time 0.0068 s, and the recognized R_s value in 0.8 s–1 s is 1.4889 Ω, with a recognition time 0.0065 s. The comparative method EKF-RMPT has a recognized R_s value of 2.9435 Ω at 0 ∼ 0.8 s with a recognition time 0.0249 s, and 1.5196 Ω at 0.8 s ∼ 1 s with a recognition time of 0.8248 s. From the above values, it can be seen that IDEEKF-RMPTC reduces the discrimination error of R_s by about 0.4 times and the discrimination time by about 0.73 times compared with EKF-RMPTC.

Figure 11 shows the graph of the result of the identification of L_s. It can be observed that its value changes from L_s to $2L_s$ in 0.6 s. From Table 5, it can be seen that the proposed method IDEEKF-RMPTC at 0 ∼ 0.6 s has an L_s discrimination value of 8.1205 mH with a discrimination time 0.0053 s, and at 0.6 s ∼ 1 s has a L_s discrimination value of 17.3036 mH with a discrimination time 0.0046 s. The comparative method

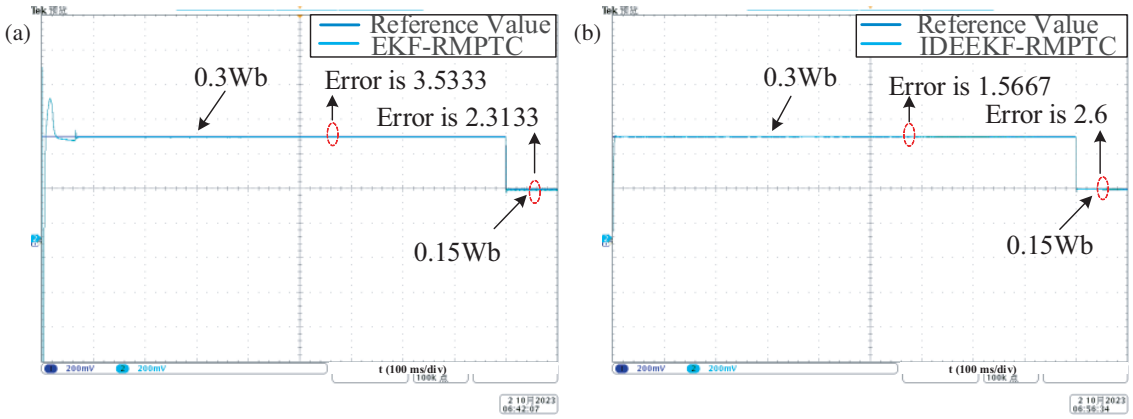

FIGURE 12. The identification result diagram of ψ_f. (a) EKF-RMPTC. (b) IDEEKF-RMPTC.

EKF-RMPT has an L_s discrimination value of 7.9308 mH at $0 \sim 0.6$ s with a discrimination time 0.0265 s, and the L_s discrimination value at 0.6 s $\sim$ 1 s is 17.3795 mH with a discrimination time 0.0320 s. By comparing the above values, it can be seen that IDEEKF-RMPTC compared to EKF-RMPTC reduces the discrimination error of L_s by 0.265 times and the discrimination time by 0.83 times.

Figure 12 shows the graph of the identification result of the magnetic flux linkage ψ_f. It can be observed that its value changes from ψ_f to $0.5\psi_f$ at 0.9 s. From Table 5, it can be seen that the proposed method IDEEKF-RMPTC has an ψ_f discrimination value of 0.3047 Wb at $0 \sim 0.9$ s with a discrimination time 0.0041 s, and the ψ_f discrimination value at 0.9 s–1 s is 0.1461 Wb with a discrimination time 0.0035 s. The comparative method EKF-RMPTC has a ψ_f discrimination value of 0.2894 Wb at 0–0.9 s with the discrimination time 0.0652 s, and the ψ_f discrimination value at 0.6 s–1 s is 0.1453 Wb with the discrimination time 0.0051 s. By comparing the above values, it can be seen that IDEEKF-RMPTC reduces the discrimination error of ψ_f by a factor in 0.34 and the discrimination time by a factor in 0.31 compared to EKF-RMPTC.

6. CONCLUSION

Aiming at the issues of high computational burden and control performance affected by motor parameters in the conventional MPTC strategy, a robust model predictive torque control strategy based on improved differential evolution extended Kalman filter is proposed. According to the analysis of theoretical research and experimental results, the conclusions are as follows:

1) The proposed RMPTC strategy uses steady-state voltage vectors to select alternative vectors. Compared with the conventional MPTC strategy, it can reduce the torque pulsation by 21.73% and stator current THD by 15.02% at rated motor parameters. *dq*-axis currents before and after the parameter mismatch as well as the speed response time are also slightly reduced.

2) The proposed IDEEKF-RMPTC introduces an improved differential evolutionary algorithm to optimize the noise matrices Q and R of the EKF. Compared with the EKF-RMPTC, the estimation error and identification time of the resistance are reduced by 37.18% and 73.24%; the estimation error and identification time of the inductance are reduced by 26.66% and 82.81%; the estimation error and identification time of the magnetic flux linkage are reduced by 34.03% and 69.71%.

ACKNOWLEDGEMENT

This work was supported by the Natural Science Foundation of Hunan Province of China under Grant Number 2023JJ50191.

REFERENCES

[1] Zhu, L., B. Xu, and H. Zhu, "Interior permanent magnet synchronous motor dead-time compensation combined with extended kalman and neural network bandpass filter," *Progress In Electromagnetics Research M*, Vol. 98, 193–203, 2020.

[2] Zhang, Y., S. Li, B. Luo, C. Luo, and Z. Yu, "Output current harmonic analysis and suppression method for PMSM drive system with modular multilevel converter," *IET Renewable Power Generation*, Vol. 17, No. 13, 3289–3297, 2023.

[3] Zhang, H., T. Fan, L. Meng, J. Guo, and X. Wen, "Polynomial estimation of flux linkage for predictive current control in PMSM," *IEEE Journal of Emerging and Selected Topics in Power Electronics*, Vol. 10, No. 5, 6112–6122, Oct. 2022.

[4] Liu, X., Y. Pan, L. Wang, J. Xu, Y. Zhu, and Z. Li, "Model predictive control of permanent magnet synchronous motor based on parameter identification and dead time compensation," *Progress In Electromagnetics Research C*, Vol. 120, 253–263, 2022.

[5] Liu, X., Y. Pan, Y. Zhu, H. Han, and L. Ji, "Decoupling control of permanent magnet synchronous motor based on parameter identification of fuzzy least square method," *Progress In Electromagnetics Research M*, Vol. 103, 49–60, 2021.

[6] Wang, Y., Y. Xu, and J. Zou, "Online multiparameter identification method for sensorless control of SPMSM," *IEEE Transactions on Power Electronics*, Vol. 35, No. 10, 10 601–10 613, Oct. 2020.

[7] Cheng, Z., C. Zhang, and Y. Zhang, "PMSWG parameter identification method based on improved operator genetic algorithm," *Progress In Electromagnetics Research C*, Vol. 139, 67–77, 2024.

[8] Vafaie, M. H., B. M. Dehkordi, P. Moallem, and A. Kiyoumarsi, "Improving the steady-state and transient-state performances of PMSM through an advanced deadbeat direct torque and flux con-

trol system," *IEEE Transactions on Power Electronics*, Vol. 32, No. 4, 2964–2975, Apr. 2017.

[9] Liu, S., C. Liu, Y. Huang, and H. Zhao, "Model predictive two-target current control for OW-PMSM," *IEEE Transactions on Power Electronics*, Vol. 36, No. 3, 3224–3235, Mar. 2021.

[10] Wang, Y., W. Xie, X. Wang, W. Yang, M. Dou, S. Song, and D. Gerling, "Fast response model predictive torque and flux control with low calculation effort for PMSMs," *IEEE Transactions on Industrial Informatics*, Vol. 15, No. 10, 5531–5540, Oct. 2019.

[11] Wang, Z., J. Chai, X. Xiang, X. Sun, and H. Lu, "A novel online parameter identification algorithm designed for deadbeat current control of the permanent-magnet synchronous motor," *IEEE Transactions on Industry Applications*, Vol. 58, No. 2, 2029–2041, Mar.-Apr. 2022.

[12] Wang, Q., G. Wang, N. Zhao, G. Zhang, Q. Cui, and D. Xu, "An impedance model-based multiparameter identification method of PMSM for both offline and online conditions," *IEEE Transactions on Power Electronics*, Vol. 36, No. 1, 727–738, Jan. 2021.

[13] Yan, L., M. Dou, Z. Hua, H. Zhang, and J. Yang, "Robustness improvement of FCS-MPTC for induction machine drives using disturbance feedforward compensation technique," *IEEE Transactions on Power Electronics*, Vol. 34, No. 3, 2874–2886, Mar. 2019.

[14] Zhang, X., Z. Wang, Z. Zhao, and M. Cheng, "Model predictive voltage control for SPMSM drives with parameter robustness optimization," *IEEE Transactions on Transportation Electrification*, Vol. 8, No. 3, 3151–3163, Sep. 2022.

[15] Zhou, Y., S. Zhang, C. Zhang, X. Li, X. Li, and X. Yuan, "Current prediction error based parameter identification method for spmsm with deadbeat predictive current control," *IEEE Transactions on Energy Conversion*, Vol. 36, No. 3, 1700–1710, Sep. 2021.

[16] Li, X. and R. Kennel, "General formulation of Kalman-filter-based online parameter identification methods for VSI-fed PMSM," *IEEE Transactions on Industrial Electronics*, Vol. 68, No. 4, 2856–2864, Apr. 2021.

[17] Li, W., G. Feng, Z. Li, M. S. Toulabi, and N. C. Kar, "Extended Kalman filter based inductance estimation for dual three-phase permanent magnet synchronous motors under the single open-phase fault," *IEEE Transactions on Energy Conversion*, Vol. 37, No. 2, 1134–1144, Jun. 2022.

[18] Zhu, M., B. Yang, W. Hu, G. Feng, and N. C. Kar, "Vold-Kalman filtering order tracking based rotor demagnetization detection in PMSM," *IEEE Transactions on Industry Applications*, Vol. 55, No. 6, 5768–5778, Nov.-Dec. 2019.

[19] Yang, R., M. Wang, L. Li, G. Wang, and C. Zhong, "Robust predictive current control of PMLSM with extended state modeling based Kalman filter: For time-varying disturbance rejection," *IEEE Transactions on Power Electronics*, Vol. 35, No. 2, 2208–2221, Feb. 2020.

[20] Qian, L., L. Sun, K. Wang, and M. Tong, "Fusion of position estimation techniques for a swing servo by a permanent-magnet synchronous machine," *IEEE Transactions on Industrial Electronics*, Vol. 70, No. 7, 6551–6562, Jul. 2023.

[21] Yang, Z., Z. Yan, Y. Lu, W. Wang, L. Yu, and Y. Geng, "Double DOF strategy for continuous-wave pulse generator based on extended Kalman filter and adaptive linear active disturbance rejection control," *IEEE Transactions on Power Electronics*, Vol. 37, No. 2, 1382–1393, Feb. 2022.

[22] Sun, X., Y. Zhang, X. Tian, J. Cao, and J. Zhu, "Speed sensorless control for IPMSMs using a modified MRAS with gray wolf optimization algorithm," *IEEE Transactions on Transportation Electrification*, Vol. 8, No. 1, 1326–1337, Mar. 2022.

[23] Sun, X., Z. Jin, Y. Cai, Z. Yang, and L. Chen, "Grey wolf optimization algorithm based state feedback control for a bearingless permanent magnet synchronous machine," *IEEE Transactions on Power Electronics*, Vol. 35, No. 12, 13 631–13 640, Dec. 2020.

[24] Wang, L., H. Guo, F. Marignetti, C. D. Shaver, and N. Bianchi, "Cuckoo search algorithm for multi-objective optimization of transient starting characteristics of a self-starting HVPMSM," *IEEE Transactions on Energy Conversion*, Vol. 36, No. 3, 1861–1872, Sep. 2021.

[25] Feng, W., W. Zhang, and S. Huang, "A novel parameter estimation method for PMSM by using chaotic particle swarm optimization with dynamic self-optimization," *IEEE Transactions on Vehicular Technology*, Vol. 72, No. 7, 8424–8432, Jul. 2023.